Geographic and Temporal Eddy Variability in the Western North Atlantic as Sensed by Satellite: An Eddy Generation Mechanism

GEORGE SEAVER

Seaver Engineering Associates Co., Cataumet, MA 02534

(Manuscript received 14 May 1986, in final form 9 March 1987)

ABSTRACT

This paper has two objectives: to establish the satellite-derived mesoscale sea surface temperature anomaly as a useful oceanographic measure and to use this measure to explore an eddy generation mechanism.

The use of satellite-derived sea surface temperature anomalies and their movement as a means of developing ocean eddy statistics is made plausible through a comparison with POLYMODE and other studies. This, plus the marked improvement in satellite resolution since POLYMODE and the use of anomaly thresholds, provides confidence in the statistical results from satellite SST. The distribution in space and time of 65 coherent eddies as sensed by satellites in the western North Atlantic is presented. The region considered is west of 50°W and the time period is March 1981 to December 1984.

A region and season of enhanced warm core eddy formation that becomes apparent from a consideration of the data is discussed, a connection is made with the seasonal interior wind stress, and an instability and generation mechanism associated with the recirculation is proposed. The shedding of warm core eddies is seen as the mechanism by which the Gulf Stream remains compatible with the gyre interior during seasonal wind stress spin-up.

1. Introduction

In the past, satellite-derived sea surface temperatures (SST) have been helpful in tracking known coherent eddies and in suggesting regions to explore for potential ones. The term eddies or coherent eddies in this paper mean a well-defined vortexlike structure, as opposed to the random, weak, background eddies referred to in Müller (1983). With the advent of the multichannel advanced very high resolution radiometer (AVHRR) in the NOAA-7 polar orbiting satellite in 1981, satellite SSTs by themselves have become useful in developing eddy statistics, as well as in exploring eddy generation mechanisms.

During the 1975 to 1978 period of the NOAA 2, 3, 4 and 5 satellites, the scanning radiometers employed only one sensing channel, made about 5000–7000 observations per day, and were calibrated once per day. This resulted in stated accuracies of ±1.5°C and spatial resolutions of 100 km. Due to atmospheric water vapor attenuation, which had spatial scales comparable to the sea surface temperature anomalies, the error was frequently as high as 4°C. These temperatures and spatial resolutions were only marginally able to resolve mesoscale eddy SST signatures. With the launching of NOAA-7 in July 1981, and the implementing of the multichannel technique for calculating SST, the water vapor attenuation problem was greatly reduced and the observation densities greatly increased. A calibration once per orbit (every 102 minutes) was also begun. These improvements resulted in an increase in the observations per day to 20 000–40 000, global coverage every three to seven days with the proper algorithm, RMSD accuracies of 0.7°C as compared with drifter buoys (Strong and McLain, 1984), temperature resolution of better than 0.5°C and probably 0.2°C in the North Atlantic, and spatial resolution of 50 km. These temperature–spatial–temporal resolutions are sufficient to resolve coherent eddy sea surface temperature signatures. This paper will investigate, in section 2, the ability of satellites to see the eddy SST signature and the eddy itself. In section 3 the eddy statistical distribution for the years 1981–84 will be presented and discussed. In section 4 the seasonal and spatial eddy distribution of section 3 will be used to investigate a particular eddy formation type, time, region, and generation mechanism associated with a Gulf Stream instability driven by the wind stress. An important goal of this paper will be to show that the shedding of warm core eddies off Cape Hatteras is a result of and a measure of wind speed variation in the gyre interior. The analogy is with the classical Strouhal experiment where the onset and frequency of eddy shedding downstream from a cylinder measures the upstream speed.

2. Eddy resolution by satellite SST

Over the last ten years there have been numerous reports in the literature of individual rings and eddies seen by satellites and confirmed by ship (Gotthardt and Potocsky, 1974; Thompson, 1984; Brown et al., 1984). Cox (1982) showed that there was a strong cor-

relation between SST and the mixed layer depth across a weak midocean warm eddy in the eastern Pacific and that this correlation was poor in the absence of the eddy. He also found that satellite imagery provided the location of the eddy boundaries with a high degree of accuracy. Richardson et al. (1978) presented for the first time a "weather map" of Gulf Stream cold core rings compiled largely from satellite observations in the western North Atlantic. Joyce (1984) in his thorough description of a warm core ring (WCR) finds, to use his words, that it is now possible to characterize the frequency of occurrence and distribution of WCRs from space without extensive shipboard measurement programs, even in the late summer. He also found a close correspondence for the ring location and shape between satellite sea surface temperature data and XBT data.

A study to show that satellites can consistently track the weaker ocean coherent eddies while rejecting strictly surface anomalies remained to be done; the POLYMODE field experiment in the North Atlantic provided the data for that study. Although Maul and Bravo (1983) attempted this comparison, their use of the data from the high altitude geostationary GOES rather than the polar-orbiting NOAA satellite produced disappointing results. Because of its single channel radiometer and, therefore, its poor ability to correct for water vapor and clouds, its lack of onboard calibration, and its poor spatial resolution, the GOES satellites are not able to resolve mesoscale eddies.

From December 1977 to May 1978 an intensive XBT program with a 20 km grid spacing was conducted in the POLYMODE area; this area was located between 26° and 36°N, 67° and 73°W. Satellite data was provided by the NOAA-5 satellite and the Global Ocean SST computation (GOSSTCOMP), a weekly gridded analysis sent by the National Environment Satellite Service (NESS) to subscribers. This analysis averaged over space and time in such a way as to minimize the effect of cloud cover and had a stated resolution of about 1°C in temperature, ten days in time, and 100 km in space (Brower, 1976). GOSSTCOMP performs a function similar to that of the human eye in looking at an infrared return from an ocean partially covered with clouds; it discriminates via thresholds between the cold return of the clouds and the cool return of the ocean and then focuses on the clear ocean SST. In doing so it sacrifices spatial resolution for better temporal coverage in cloudy atmospheres. Water vapor can affect the temperature resolution in an unknown way, but the relative nature of the temperature requirement here makes this less of a problem. A satellite SST anomaly was considered a candidate for an eddy SST signature if the isotherm was a mesoscale closed contour and 1°C or more above or below the background. Although the individual SST signatures were, consequently, sometimes speculative, their movement was not. The results of the comparison with POLYMODE were reported in Seaver (1979) and revealed that 90% of the eddies had a SST signature during at least part of their lifetime that was observed by research vessels, and 100% of the eddies whose 15°C isotherms were displaced greater than 75 meters showed a surface anomaly. Furthermore, there were no mesoscale SST signatures that lasted for two weeks or more that did not have an eddy structure beneath them. The satellite analysis resolved 56% of all of the eddies and 71% of those with a 15°C isotherm displacement greater than 75 meters. A similar multiship XBT survey in the eastern North Atlantic (between 32° to 42°N, 20° to 60°W) showed that one-third of the eddies had a SST expression and that the eddies were considerably weaker than those in the west (Emery et al., 1980).

This rather lukewarm endorsement of the satellites' ability to resolve mesoscale eddies is strengthened by the introduction in 1981 of the multichannel radiometer and processing algorithm mentioned previously. Figure 1 presents a simultaneous comparison of the GOSSTCOMP 100 km analysis previously used and the present 50 km analysis; a 1°C mesoscale SST anomaly in the 100 km analysis translates into a 2°C and even 3°C anomaly in the 50 km analysis. It is the author's opinion, as supported herein, that the current analysis will allow all coherent ocean eddy SST signatures that can be resolved by ship SST to be seen by satellite during at least part of their lifetime.

A more recent but limited study of the kinematical interpretation of satellite SST obtained from the multichannel radiometer is presented in Hardtke and Meincke (1984) for the eastern North Atlantic between 20°W and 50°W and 40°N and 55°N. They found that for the weaker eddies of the eastern North Atlantic and during the wintertime there was a high correlation between the satellite SST and drogue measured currents; they also found that for two out of three of the two-week summertime comparisons there was a high satellite to drogue correlation. The correlation decreased in the one comparison where the seasonal thermocline was greater than 0.25°C m^{-1}. In addition they found that, although the satellite SST (skin temperature) was up to 0.5°C greater than the bulk SST as measured by ships, the satellite SST tracked the near surface temperature accurately.

3. Eddy statistics from satellite SST anomalies for the period 1981 to 1984

Weekly GOSSTCOMP SST charts have been available since 1978, although only those charts produced since the introduction of the multichannel radiometer technique and the 50 km analysis in March 1981 have been used here.

The SST features that we catalogued for this study were mesoscale size closed isotherms (100 to 400 km), at least 2°C above or below the background temperatures, that lasted for three analyses, two weeks or more.

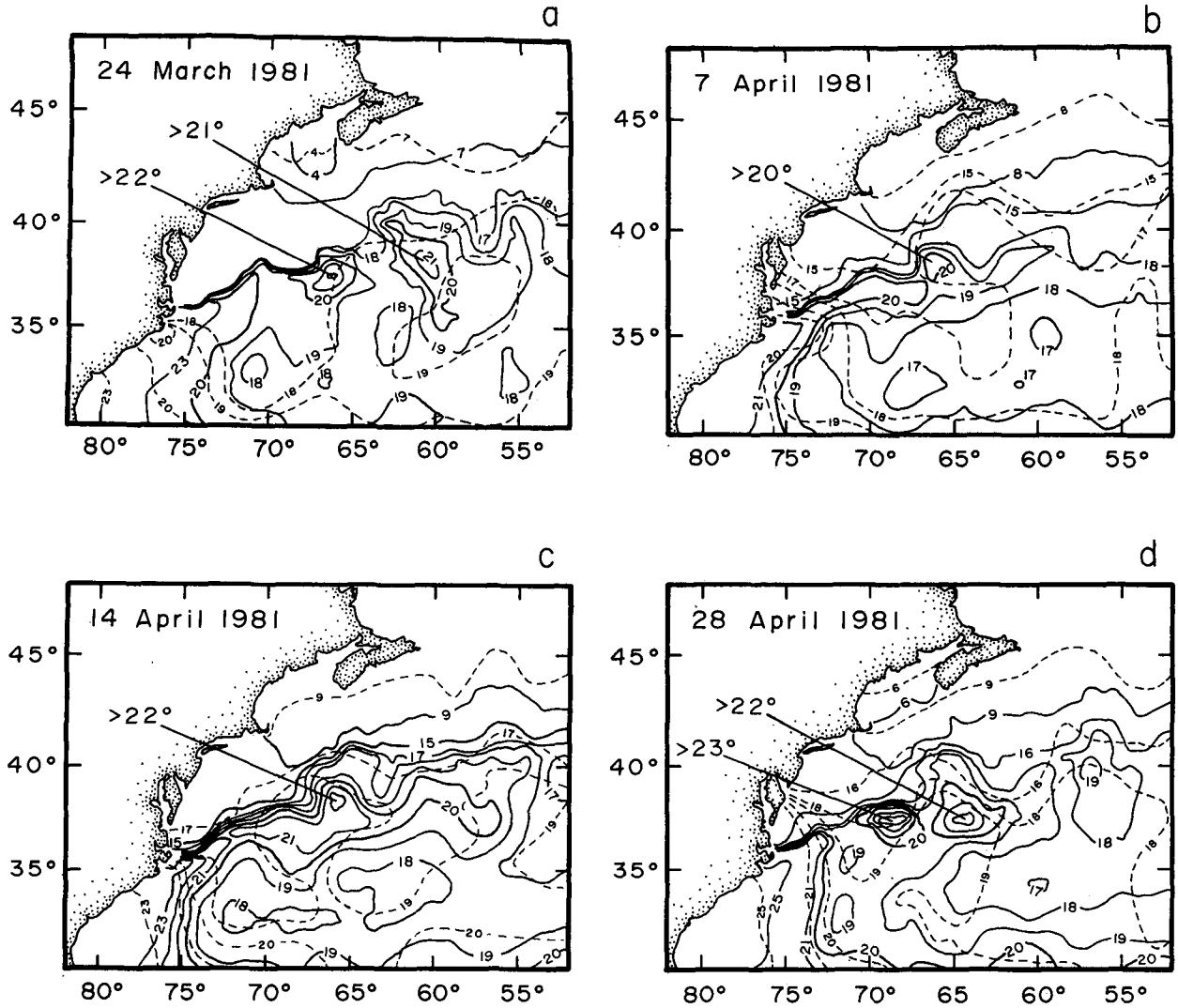

FIG. 1. NESS GOSSTCOMP sea surface temperature analysis. Solid lines represent the 50-km analysis and dotted lines represent the much less detailed 100-km analysis of the western North Atlantic. The 100 km analysis barely resolves the mesoscale SST. The sequence also shows the development of Gulf Stream/south warm core eddies and countercurrent, possibly from Gulf Stream/countercurrent instabilities.

The observation area is that of the 50 km resolution chart; that is, from the coast of North America east to 53°W. The time of the study is from 24 March 1981 to 30 December 1984. The 2°C and two-week thresholds were imposed to exclude weak and surface disturbances, and to insure that only coherent eddies are catalogued. Basically, these thresholds are a "dynamically important" criterion. The observed movement of these satellite-derived mesoscale SST anomalies acts as a geostrophic filter, as described in Emery et al. (1986). They found that the satellite-derived advective movement of the SST anomaly over an eddy agreed with the near surface CTD-derived geostrophic velocity, and that agreement was poor elsewhere. Under the above constraints we observed a total of 43 eddies seaward of the Gulf Stream, hereafter called GS/S, and 22 eddies on the north side, hereafter called GS/N; their geographic distribution and mean tracks are shown in Fig. 2. Disturbances which remained attached to or in the Gulf Stream were not tabulated here.

On the south side of the Gulf Stream 70% of the eddies were found and remained in an area 1100 km along and 550 km out from the stream (an area outlined in Fig. 2), as we might have expected. This compares with the North Atlantic surface drifter data of Richardson (1983) who found that the *e*-folding scale for the eddy kinetic energy (the 37% point) extended out 300 km from the Gulf Stream (along 65°W). From Halkin and Rossby (1985) we infer that two-thirds of the "eddy" energy near the stream is actually from meanders, so that Richardson's *e*-folding scale for strictly eddy kinetic energy would then be close to 600 km. This is obtained from Richardson's Fig. 11b (1983) by reducing its peak kinetic energy by two-thirds. The

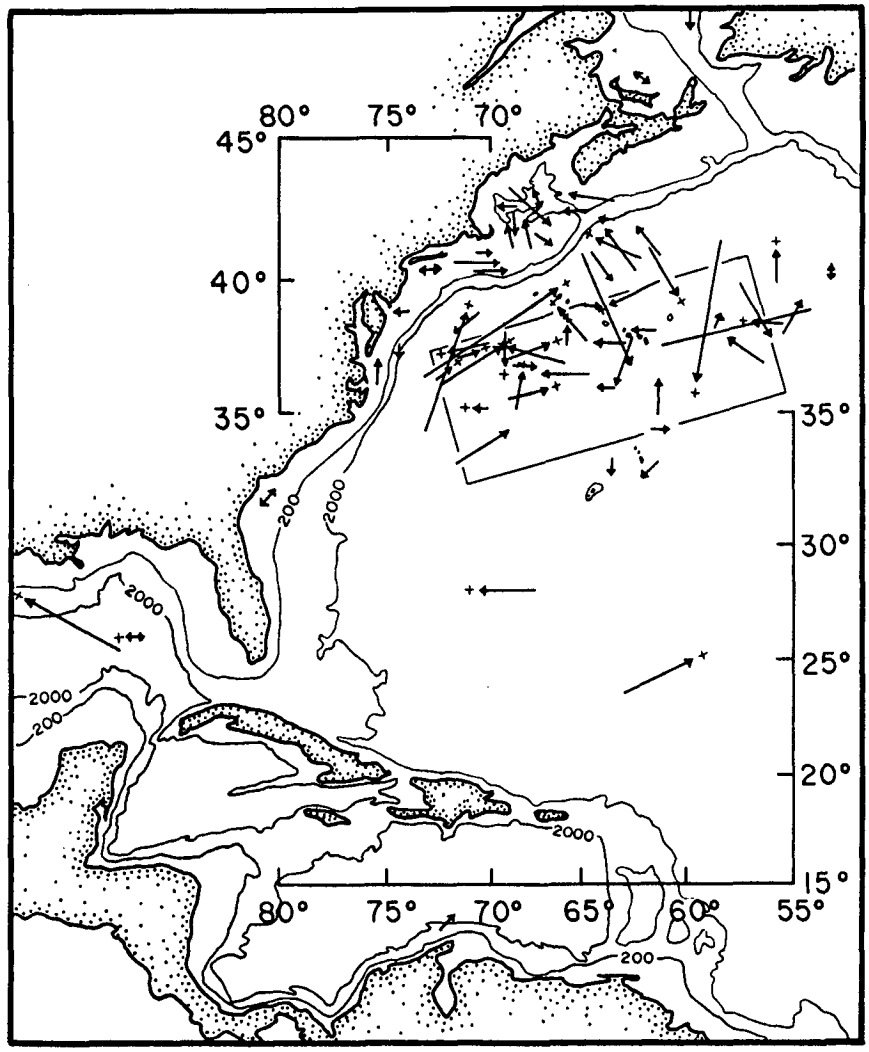

FIG. 2. Geographic distribution and mean tracks of the mesoscale SST anomalies as observed by NOAA-7 satellite and the GOSSTCOMP 50-km analysis for the period March 1981 to December 1984. Arrows pointing in both directions indicate oscillatory movement, and the box indicates a region of enhanced seasonal eddy production as discussed in the text. The symbol "+" at the end of the arrow for GS/S eddies indicates a WCE.

comparison of Richardson's *e*-folding scale with the present *e*-folding of 550 km is valid if the average kinetic energy per eddy does not change moving away from the Gulf Stream.

In the Gulf of Mexico two loop current rings were observed, as well as a cold core eddy off the Lake Maricaibo estuary in Venezuela. The term "ring" as used here means an eddy that was observed to pinch off from the Gulf Stream system.

On the north side of the stream the distribution was more uniform with eddies associated with the runoffs from the Savannah, Chesapeake, Delaware, Hudson, and St. Lawrence rivers (27%). There were also rings from the Gulf Stream, as well as other eddies associated with the shelf circulation. In general, there was quite a diverse collection of mesoscale disturbances.

The mean size of the GS/S eddies was 215 km with a mean speed of 4.0 km day^{-1}, a mean track length 190 km, and a mean lifetime of 56 days. In the case of the GS/N eddies their mean size was 146 km with a mean speed of 1.1 km per day, and a mean track length of only 61 km reflecting, presumably, their more confined region for movement. The mean lifetime of GS/N eddies was 76 days. The mean track lengths and lifetimes for all eddies were probably underestimated by the SST signature longevity; that is, the eddy formation data of Figs. 3a, f and 4a are correct, but the eddy population data of Fig. 3b–e and 4b–e are underreported, at least for August and September. Some eddies were observed to reenter the Gulf Stream; however, others simply disappeared for no apparent reason. GS/N eddy 9 from Table 1 existed for 252 days, whereas in Joyce (1984) the same eddy was observed for about 345 days. These properties and others are

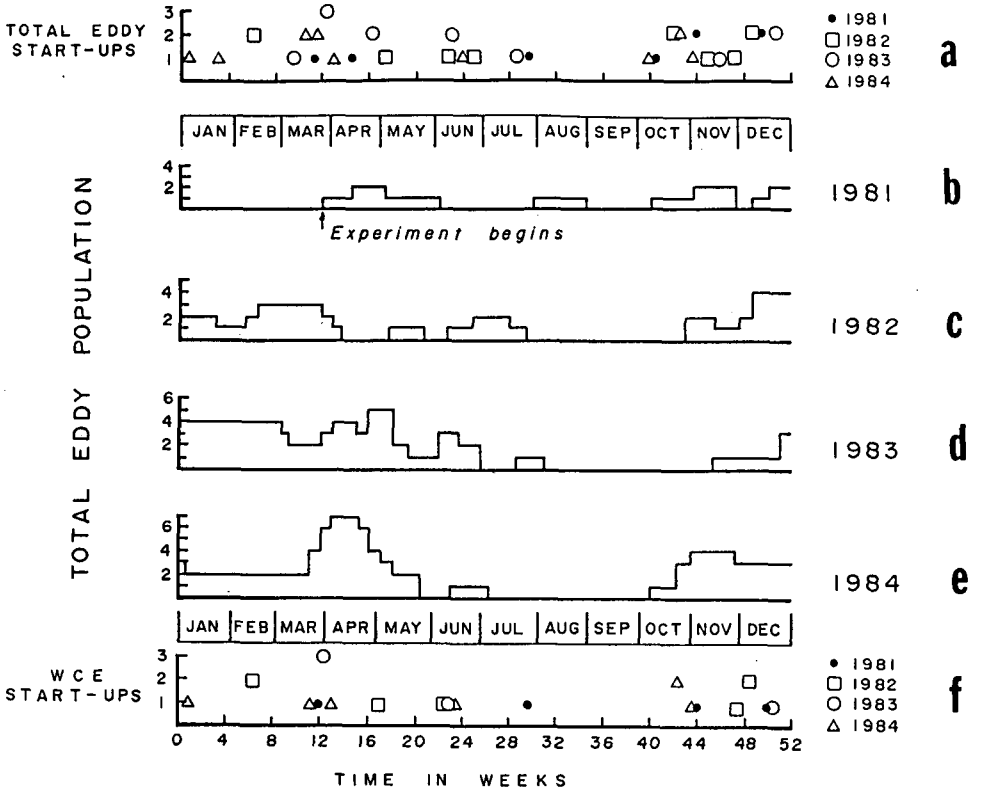

FIG. 3. Gulf Stream/south eddy distribution in time and by eddy type for the region bounded by the Gulf Stream, 53°W, South America, and Mexico and for the period March 1981 to December 1984. (Top) New eddy formations for all types (CCE, WCE, CCR); (middle) residential eddy populations for all types for the years 1981–84; (bottom) warm core eddy formations for the years 1981–84.

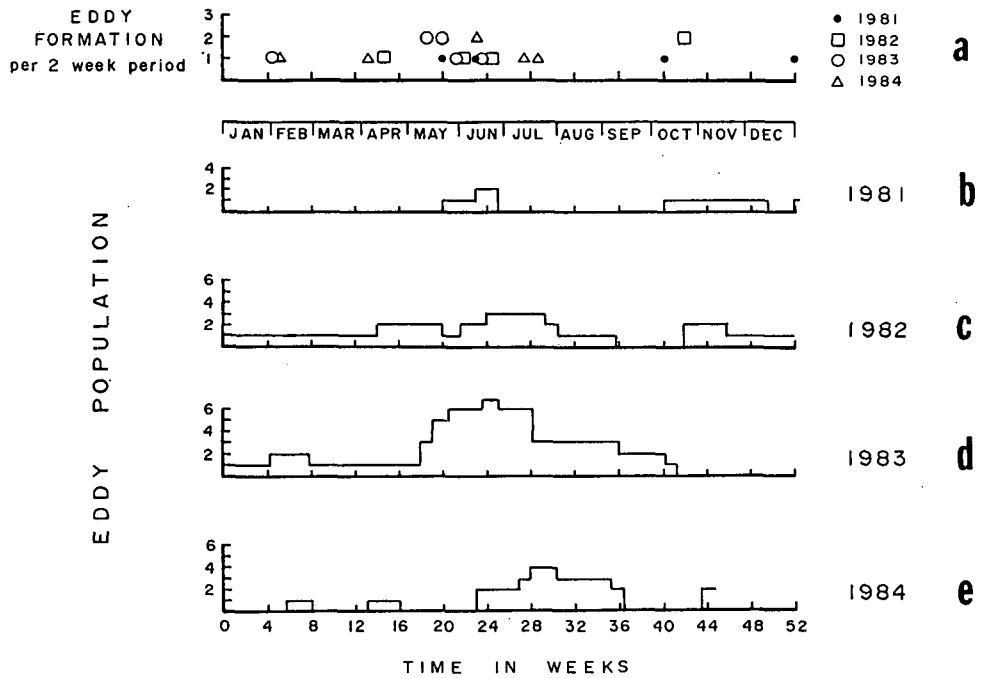

FIG. 4. Gulf Stream/north eddy distribution over time for the region bounded by the inshore edge of the Gulf Stream, the coasts of Canada and the United States, and 52°N latitude for the period March 1981 to October 1984. (Top) New eddy formations per two-week period for all types (CCE, WCE, WCR); (middle) residential eddy populations of all types for the individual years 1981 to 1984.

TABLE 1. Location, size and drift of satellite GOSSTCOMP mesoscale anomalies for the western North Atlantic during the period 1981–84.

Eddy number	Eddy type	Central temperature		Temperature above/below amb. (°C)	Size (km)	Date		Lat/long		Lifetime (days)	Drift speed (km d^{-1})	Direction/ track length (km)
		Begin	End			Begin	End	Begin	End			
						a. Ocean eddies or GS/S						
1	WCE	22	22	+4	287	3/24/81	6/2/81	37/66	37.5/69	70	3.3	W/230
2	CCE	18	18	−1	183	4/14/81	5/5	33/72	34/69	21	15	NE/319
3	WCE	28	26	+1	172	7/28	9/1	37.5/66	38/66	14	1.2	N/17
4	CCE	25	22	−1	192	10/13	10/27	37/57	38/58.5	14	10.4	NW/146
5	CCE	21	21	−1	240	11/3	11/24	38/62	38/63	21	5.3	W/110
6	WCE	22	22	+1	146	11/3	11/24	40/62	39/64	21	9.8	W/205
7	CCR	19	17	−3	300	12/8/81	1/26/82	38/63	36/64	39	6.6	SSW/257
8	WCE	20	21	+3	377	12/15/81	4/6/82	37/69	37.5/66.5	63	4.4	E/277
9	WCE	18	18	+2	120	2/9/82	3/30/82	38.5/56	38.5/57.5	49	2.5	WSW/123
10	WCE	22	21	+3	137	2/16	3/23	36/72.5	36.5/72	35	2.5	E/88
11	WCE	26	25	+2	270	5/4	5/25	24/63	25/60	21	14.3	ENE/300
12	WCE	25	26	+2	190	6/8	7/13	36/72.5	37.5/69.5	35	8.1	ENE/284
13	CCR	17	21	−4	140	6/22	7/27	39/65	39/65	35	0	—
14	CCE	22	21	−2	240	10/24	11/9	38/59	38/59	16	1.6	NNE/26
15	CCE	23	23	−2	213	10/24	11/9	34.5/62	34.5/62	16	2.8	E/45
16	CCR	20	17	−4	206	11/9/82	3/1/83	36.5/65	36.5/67.5	112	2.0	W/224
17	WCE	26	22	+2	314	11/30/82	4/19/83	25.5/87.5	28/92	140	3.9	WNW/550
18	WCE	22	21	+2	223	12/7/82	3/8/83	38/69	37/69	91	1.2	SSW/110
19	WCE	23	21	+2	163	12/7/82	3/8/83	37/72	37.5/71	91	1.1	NE/100
20	CCE	16	17	−3	275	3/8/83	3/29/83	33/62	32.5/62.5	21	2.2	SW/46
21	WCE	20	20	+2	115	3/29	5/3	35/70.5	35/71	35	0.7	W/25
22	WCE	20	20	+2	155	3/29	5/3	35.5/68.5	37/68.5	35	4.4	N/154
23	WCE	25	25	+3	347	4/5	5/3	26/87	26/87	28	0	—
24	CCE	22	22	−5	338	4/26	5/17	13/72	13.5/71.5	21	3.5	NE/74
25	CCR	11	13	−4	194	4/26	6/14	40.5/53.5	40.5/53.5	49	0	—
26	WCE	27	26	+2	303	6/7	6/28	28/67.5	28/70	21	1.9	W/40
27	CCE	22	24	−2	201	6/7	6/28	33/64.5	32/64.5	21	3.6	S/76
28	CCE	22	22	−3	137	7/19	8/2	36/64	36/64	14	1.8	W/25
29	CCR	16	19	−2	206	11/15/83	1/24/84	41.5/59	36.5/60	70	7.7	S/540
30	CCR	18	17	−2	210	12/20/83	1/3/84	38/56	39/56	14	3.7	NE/52
31	WCE	21	21	+2	183	12/20/83	1/3/84	40/58	38/57	14	16	SE/224
32	WCE	24	22	+3	206	1/3/84	4/17/84	37.5/70	37/72	104	2.2	W/232
33	CCR	13	19	−2	223	1/24/84	5/22/84	39/55	37.5/62	118	5.5	WSW/650
34	WCE	21	21	+3	206	3/20/84	4/24/84	37.5/65.5	38.5/67	35	5.4	NW/190
35	CCR	14	19	−4	275	3/20	5/22	38/63	38/64	63	1.8	W/113
36	CCE	18	19	−2	195	3/27	4/24	35/62	36/62	28	4.9	N/137
37	CCR	14	20	−4	257	3/27	5/1	37/68.5	37/68	35	3.7	E/130
38	WCE	21	23	+2	225	4/3	5/8	35.5/69	36/67.5	35	2.2	E/77
39	WCE	22	23	+2	216	6/12	7/3	40/56.4	41/56.4	21	4.8	N/100
40	WCR	26	24	+2	210	10/21	11/27	41/62	39/60.5	37	5.4	SE/200
41	CCR	17	18	−3	116	10/9	4/22/85	41/65	37/63	195	2.3	SSE/450
42	WCE	26	25	+2	180	10/23	7/1/85	36/73	39.5/66	251	2.5	NE/625
43	WCE	26	26	+2	170	10/30	7/1/85	34/74	38/71	244	1.8	NNE/450
						b. GS/N						
1	CCE	12	18	−1	64	5/19/81	6/23/81	41/68	42/68.5	35	1.6	NW/56
2	WCE	14	16	+1	55	6/9	6/23	43/67.5	43/67.5	14	0	—
3	CCE	22	11	−2	154	10/6	12/15	37.5/74.5	37.5/74.5	70	0.25	S/18
4	CCE	19	20	−5	189	12/29/81	9/7/82	32/80.5	32/80.5	252	0	—
5	WCR	15	15	+2	103	4/13/82	5/18/82	39/70.5	38/72	35	4.5	SSW/165
6	WCE	3	14	+2	188	6/1/82	8/3/82	49/60.5	49/60.5	63	0.4	S/29
7	WCE	10	16	+2	306	6/22	7/27	42.5/68.5	42.5/69	35	0.7	W/25
8	CCE	13	12	−2	81	10/19	11/16	41/70.5	41/70	28	1.2	E/34
9	WCR	24	16	+3	145	10/19	6/28	40.5/63	42/64.5	252	0.8	NW/193
10	CCE	11	8	−2	146	2/1/83	2/22/83	36/75.5	37/75.5	21	3.2	N/67
11	CCE	5	14	−2	255	5/10	9/13	43/64	43/66	126	1.0	WNW/120
12	CCE	6	15	−2	81	5/10	10/11	41/71	41/69.5	154	0.8	E/123
13	CCE	6	15	−2	66	5/17	7/19	40.5/73	40.5/73	63	0	—
14	CCE	8	20	−2	86	5/17	7/19	39/74	39/74.5	63	0.5	W/32
15	CCE	6	13	−2	160	5/24	7/19	43/69	42/67	56	3.7	SSE/207
16	WCE	11	15	+3	178	6/14	10/18	42/68	41.5/67.5	126	0.8	SE/97
17	WCR	8	8	+2	190	2/7/84	2/28/84	42/64	42/64	21	1.9	W/40
18	CCE	5	5	−1	120	4/3	4/24	41/69	42.5/69.5	21	0.8	N/15
19	CCE	6	12	−3	160	6/12	9/11	43/66	43/66	91	0.3	W/24
20	CCE	11	18	−3	127	6/12	9/11	41/70.2	41/69	91	0.7	E/64
21	WCE	18	20	+3	223	7/10	9/4	42.5/69	42/68.5	56	0.6	S/34
22	WCE	18	17	+2	132	7/17	7/31	47/63	47/63	14	0	—

tabulated for all 65 eddies in Table 1; the directions and speeds of eddy propagation are highly variable with no single theme discernible to this observer.

Joyce (1984) reports an annual formation of eight WCRs per year in the period 1976–80 for the GS/N. This is significantly higher than the three per year reported here (one as a WCR and two as WCE). In this study we did not include rings that did not have at least three sightings (two weeks) and appear on the north side of the Gulf Stream, since SST signatures of possible rings that remained close to the Stream appeared too ambiguous. Also small rings that remained close to the Stream might not be depicted as separate entities by the GOSSTCOMP analysis. There is a trade-off between resolution in space and time, and coverage with partial cloud cover that is maintained by the GOSSTCOMP procedure.

The eddy distributions over time and type for the years 1981 to 1984 are presented in Figs. 3 and 4. The results for 1981 are incomplete and less energetic than later, as the routine 50 km analysis started in March and the full multichannel input did not start until November 1981. There was an average of 12.3 coherent eddies generated per year in the area bounded by the Gulf Stream, 53°W, South America, and Mexico (GS/S), with 88% of them beginning in the spring or fall, as shown in Fig. 3a. Furthermore, the eddy populations from Fig. 3d, e reach a maximum in April/May. This compares with the surface drifter analysis of Richardson (1983) who observed a noisy peak in May. The noise in his case was probably caused by his limited number of degrees of freedom and the contamination of the eddy kinetic energy with spatial gradients and Gulf Stream meandering. Halkin and Rossby (1985) found meanders to account for two-thirds of the surface velocity variability in the vicinity of the stream.

Of the 12.3 GS/S eddies observed to form per year, 24% were cold core rings, 29% were cold core eddies, and 47% were warm core eddies. The three CCR and four CCE per year found in this study compare with the five to eight CCR per year formation rate estimated by the Ring Group (1981). On 4 April 1982 El Chichón volcano in Mexico (17°N, 93°W) erupted; the debris from this volcano immediately began to affect satellite SST accuracy and reliability in the regions downwind in the Pacific. By May 1982 the satellite SST retrievals had been reduced by two-thirds in the North Atlantic subtropical gyre (Strong et al., 1982). By the summer of 1983 the effects of El Chichón had diminished considerably (Strong and McLain, 1984), although they had also spread to higher latitudes. By observing the eddy formation and eddy populations of Figs. 3a–e, we see that El Chichón did not have a significant effect in this study. In fact, Fig. 3c–e indicates an increase in GS/S eddy population for late 1982 and 1983 and an increase in GS/N eddy population for mid-1983 (Fig. 4d). This is gratifying to know as it suggests that the technique is robust to changes in atmospheric aerosols.

From Fig. 3b–e we note that the eddy population consistently goes to zero in the late summertime North Atlantic, suggesting a possible masking effect by the seasonal mixed layer (from high insolation and light winds). However, a number of investigators have tracked weak eddies in the late summer by satellite (Tabata and Gower, 1980; Ikeda et al., 1984). Specifically regarding seasonal mixed layer heating in the open ocean, as mentioned previously, Hardtke and Meincke (1984) found a high correlation between the SST and drogue velocities except when the seasonal thermocline was greater than $0.25°C\ m^{-1}$ and the eddy was weak. Further, a look at the GS/N eddy SST statistics of Fig. 4 reveals that the maximum satellite-sensed activity north of the stream is in the summer. The satellite-sensed formation of GS/N eddies continues through July, and the eddies retain a SST signature through August and, in 1983, through September, whereas the GS/S satellite peak is in April. Also, high insolation and light winds could not explain the midwinter dip in satellite eddy SST activity shown in Fig. 3.

Finally, in regards to summertime masking of the eddy SST signature in the eastern North Atlantic, Emery et al. (1980) conducted a multiship XBT survey between 32° and 42°N from 20° to 60°W. They found the greatest number of eddies in their spring swath and the least in their July swath. More importantly, in July, 50% of the eddies had a SST, whereas the overall December to July figure was 33%. The eddies they observed were weak compared with those west of 60°W, with isotherm displacements two to three standard deviations of the overall isotherm variation.

A useful comparison can be made by comparing the POLYMODE results of December 1977 to May 1978 with the average results generated here for the same region and season. There were nine eddies observed in POLYMODE; the average for the 1981–84 period here from Table 1 is seven eddies in the December to May time frame. Two of the POLYMODE eddies were weak with less than a 75 meter displacement of the 15°C isotherm (POLYMODE XBT Group, 1978, 1979).

In another study Cornillon et al. (1986), using satellite SST data from the period 1979 to 1984, catalogued eighteen warm water "outbreaks" of the Gulf Stream into the Sargasso Sea. These events have a surface expression of up to 3.3°C, and disappear in less than ten days. These outbreaks are of the order of 100 km in size and are observed between 67° and 72°W; their vertical extent is unknown, but a 100 meter depth is a good guess. Their region of appearance is somewhat east of the major formation region of our WCEs. The two-week observational criterion used for the present analysis would, at any rate, eliminate them from being catalogued in this survey.

Finally, the temporal eddy distributions for the GS/N region are presented in Fig. 4a–e; this region is the area bounded by the Gulf Stream and the coast to the

west. There was an average of 7.3 eddies per year generated in this region with 64% of them appearing in the early summer (middle May to middle July). Of the total, 14% were warm core rings, 27% were warm core eddies, and 59% were cold core eddies. Every year in May or June there was an abrupt onset of shelf eddying with no start-up appearing after the third week in July; this is shown in Fig. 4a.

Using the mean eddy sizes of 146 and 215 for GS/N and GS/S eddies respectively, the average occupancy rate for GS/N is 8.6%, and for the North Atlantic subtropical gyre west of 53°W it is 2.6%. The occupancy rate was determined by calculating the eddy-years from Table 1 and dividing into this the close-packed eddy capacity for the given area. If we consider an area starting due east of Cape Hatteras and extending 1100 km along the Gulf Stream (72° to 58°W) and 550 km seaward of it, we would encompass a region of much greater eddy density, as shown in Fig. 2. This region has an average annual occupancy of 8% and from Table 1 an occupancy rate in April 1984 of 56%; however, because of the potential masking of the eddy SST in July and August the 8% mean should be viewed with caution. In a similar way the occupancy rate for the GS/N region in July 1983 is 35%. The occupancy rates for the peak eddy seasons cannot become much larger than what is reported here.

4. Eddy generation

a. Dynamical wind–eddy relationship

Two of the surprising results of the previous section are that 59% of the eddies produced on the north side of the Gulf Stream are cold core and 47% of those observed in the south side are warm core. An instructive satellite SST chart in color showing the various eddy types can be seen on the back cover of the winter 1986/87 issue of *Oceanus*. The period is the first week of April 1984 and provides the context for the data of Figs. 3 and 4 for the spring of 1984. This period has the highest eddy population of any during this study. Given the known Gulf Stream ring generation mechanisms, we might expect warm core eddies to predominate in the north and cold core in the south. Further, as we can see in Fig. 3f of the southern WCE formation through the years, 30% of them appear in the last two weeks of March. This along with the July–August minimum from Fig. 3 suggests a wind related generation.

Müller (1983) characterizes the oceanic synoptic scale variability as, to use his words, consisting of a random, low-level, homogeneous background field that is atmospherically forced, and on which are superimposed well-defined energetic eddies, rings, and meanders that are caused by current instabilities. Dickson et al. (1982) find the random eddies of the eastern North Atlantic also coherent with the wind stress and nearly in phase with it, particularly near the surface; the eddy kinetic energy in Dickson is generated during the late winter and early spring, propagates to abyssal depths, and decays to a minimum in late summer. It also reflects the January/February dip in the local wind stress. In the present study of the western North Atlantic we find that the formation of large amplitude eddies, whose distribution in time is shown in Fig. 3, is also in phase with the wind stress, but the wind stress of the gyre interior.

In Fig. 5 the monthly wind and wind stress at Bermuda and for Marsden Square 114, (MS 114 center at 35°N, 55°W) are shown for the years 1980 to 1984. The Bermuda winds were obtained from NODC (M. Briscoe, private communication), and the MS 114 data is from NCDC, Asheville, North Carolina. The latter is compiled as the surface marine observations, tape deck 1129 (TD 1129). Figure 5a presents the monthly averages for the east–west wind stress component over the northern half of MS 114 (35°N to 40°N and 50°W to 60°W) over the years 1980–84. The wind stress was calculated using a modified version of Bunker and Goldsmith's (1979) procedure. Figure 5a shows peaks in November and March with a midwinter minimum in December. There is also a deeper, broader summer minimum from May through October. Also shown in Fig. 5a by the arrows are the beginning and end of the fall and winter WCE formation periods, as taken from Fig. 3f. There is an approximate correlation between the wind stress peaks and lulls and those of the WCEs, although the WCEs continue to form in the spring two months after the wind stress has begun to diminish.

The monthly averages of the east–west wind stress component for the individual years 1980–84 are shown in Figs. 5b–f and are more revealing. The arrows now indicate the onset and end of the warm surface core of water (Worthington, 1977) on the southern edge of the Gulf Stream that precedes the WCE formation. This we will call the seasonal near-stream recirculation or countercurrent, and it is determined from an examination of the weekly 50 km satellite SST analysis. Several examples of this countercurrent are shown in Figs. 1b and 6b, d, f and k; they are comprised of "U" shaped isotherms that turn back on themselves and ultimately appear to spawn and envelop the WCEs along the southern edge of the Gulf Stream (a dynamic topographic ridge).

For the year 1980 shown in Fig. 5b, the magnitude of the wind stress (symbols) has been plotted along with the east–west component (line); there is a significant difference in these only for the June through September period. The east–west component will be the only one considered in this study. For 1980 the southern half of MS 114 has about two-thirds the wind stress of the northern half but it is similar in form. There is no Bermuda wind data available for 1980. The wind stress (τ_w) for MS 114 exhibits significant peaks in February and November of ~0.35 Pa (3.5 dyn cm^{-2}), with a December lull down to one-quarter of the peak value. The satellite SST data for this period was from a single

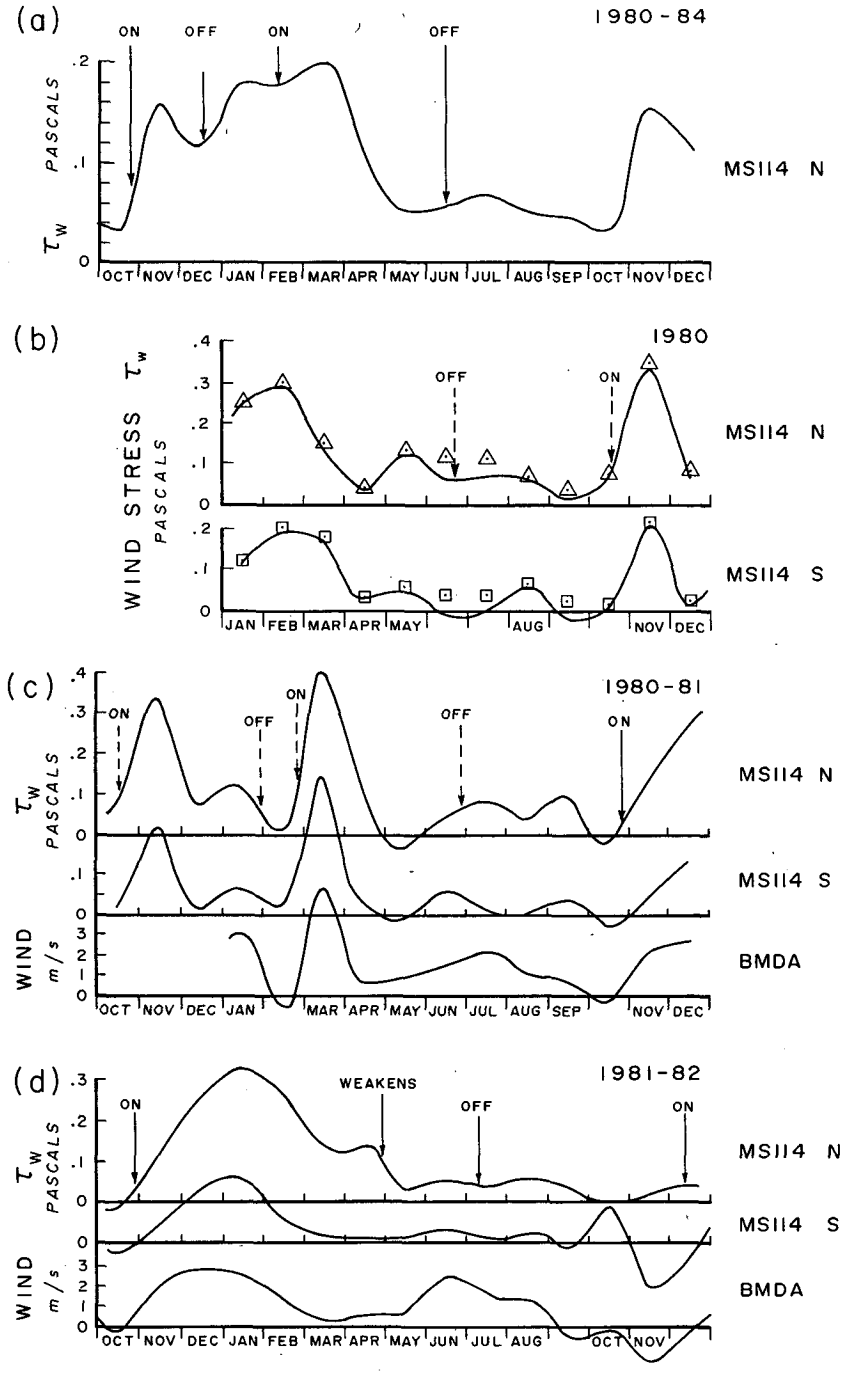

FIG. 5. The average monthly wind and wind stress over the North Atlantic for the period 1980 to 1984. The Bermuda wind is from NODC for the period 1981 to 1984. The wind data for the northern and southern halves of Marsden Square 114 (MS114/N and MS114/S) is from NCDC, TD 1129. MS114 covers 30° to 40°N, 50° to 60°W. (a) The monthly averages for MS114/N of the east-west wind stress component over the years 1980–84. The arrows indicate the beginning and end of the WCE formations taken from Fig. 3f. (b) The monthly averages for MS114/N and MS114/S of the wind stress magnitude (symbols) and east-west component (line) for 1980. Bermuda wind data is not available for 1980. The dotted arrows indicate the status of the countercurrent south of the Gulf Stream, as derived from the 50 km GOSSTCOMP satellite charts (the single channel analysis). In mid-June the countercurrent turns off and in mid-October it turns on again. (c) The monthly averages of the east-west wind stress for MS114/N and MS114/S and the winds for Bermuda for 1980–81. The arrow indicates the status of the countercurrent south of the Gulf Stream, as derived from the satellite SST charts. The dotted arrows indicate data from the single channel analysis. The multichannel analysis commenced in October 1981. (d) As in (c) except for 1981–82. (e) As in (c) except for 1982–83. (f) As in (c) except for 1983–84. The data for the status of the countercurrent was taken from the satellite charts of Fig. 6a–k.

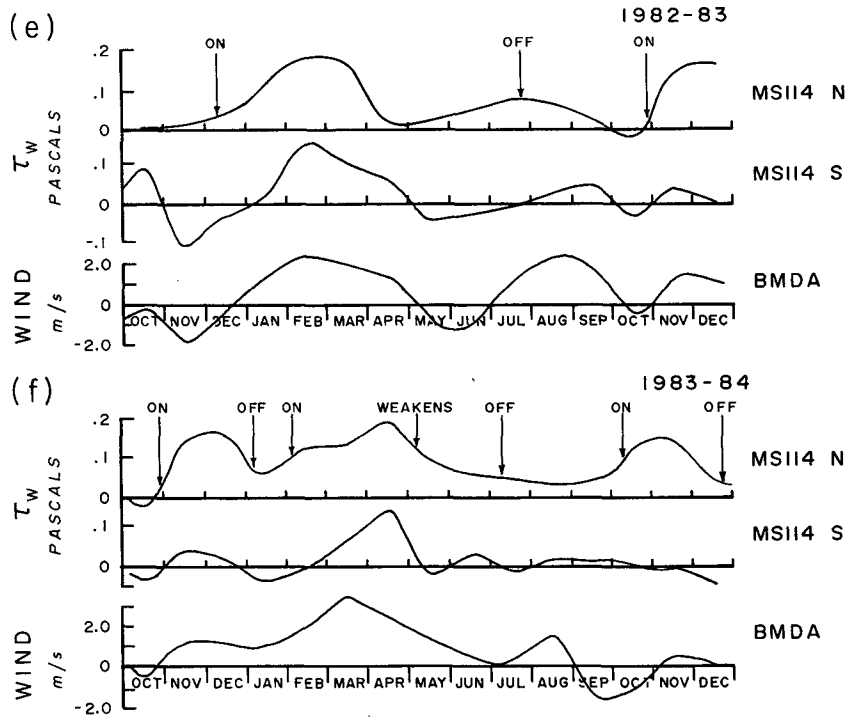

FIG. 5. (*Continued*)

channel radiometer and computation, and was not used to compile the eddy statistics of Table 1 and Figs. 3 and 4; however, the satellite data has been used to establish the status of the countercurrent for 1980 and 1981. The summer 1980 end to the countercurrent occurs in the third week of June, and the fall onset occurs in the third week of October, when τ_w reaches 0.07 Pa.

For 1980–81 (Fig. 5c) we again only have single channel satellite SST data for the first nine months of 1981, but we have the Bermuda winds for all of 1981. We have not presented the wind stress at Bermuda because we did not know the drag coefficient as a rule; we were able to estimate it for the March 1981 peak, which gave a value (0.1 Pa) of about one-quarter that of MS114/north and one-third that of MS114/south. The monthly variation of all three were similar; the peaks occurred in November and March with a broad, deep lull from December through February going down to 2% of the peak value. The winter lull in the countercurrent occurs in the last week of January, when τ_w drops below 0.05 Pa, and the countercurrent returns in the last week of February when τ_w rises above 0.07 Pa. The summer end occurs in the last week in June. Why the countercurrent does not turn off in the last week in April, when τ_w drops below 0.05 Pa (as is the case in January), remains an inconsistency. The fall onset of the countercurrent occurs at the end of October when the wind stress rises to 0.04 Pa or 12% of the subsequent January peak value; the onset occurs over a period of 1–2 weeks.

For 1981–82 (Fig. 5d) we have data for MS 114, Bermuda, and the multichannel satellite SST, and are better able to test the dynamic link between the wind stress and the WCEs. The wind stress for MS 114/N has a broad peak between October 1981 and March 1982 centered on January 1982. There is only a weak wind stress lull (March) and second peak (April), and this is reflected in the countercurrent; it does not have a readily identifiable change. However, at the end of April it does noticeably diffuse when the wind stress drops below 0.1 Pa, and stops altogether in July when τ_w drops below 0.05. The countercurrent returns again in the fall (December) when τ_w exceeds 0.04 Pa. The τ_w of MS114/S more nearly reflects the features of the Bermuda wind than those of MS114/N. The January peak τ_w of MS114/N is 230% that of MS114/S; more importantly, the monthly change in the wind stress difference between MS114/N and MS114/S ($\propto \nabla \times \tau_w$) generally follows the monthly change in τ_w of MS114/N. The wind stress curl is important, as it drives the mean circulation changes. A thorough investigation of the mean monthly wind stress curl variation awaits the reduction of TD1129 for the other Marsden Squares (111–116).

For 1982–83 (Fig. 5e) we have wind and WCE data for the full year; it is quantitatively different from other years or the mean and this difference shows up in both

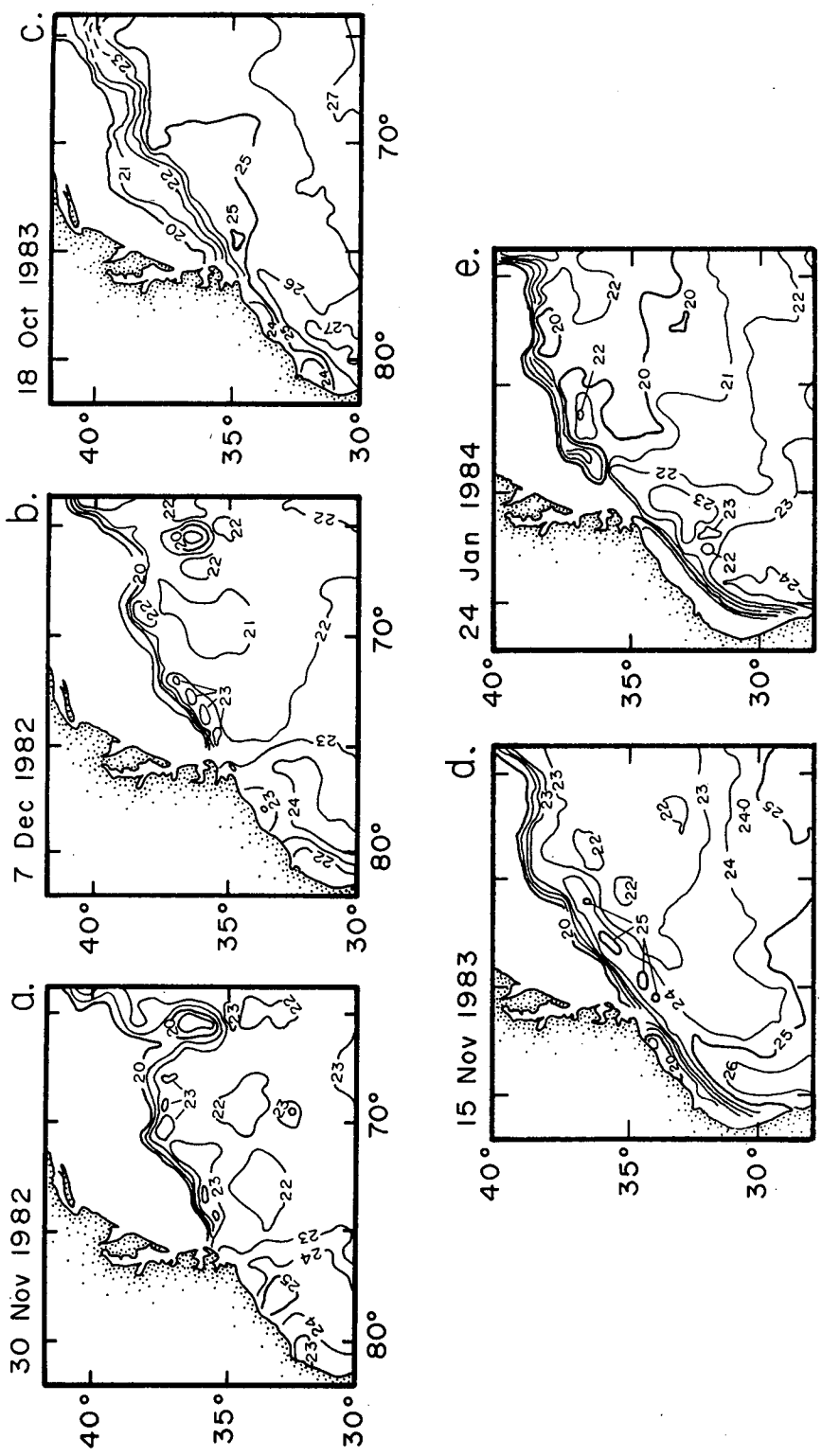

FIG. 6. Satellite GOSSTCOMP charts of the Gulf Stream and countercurrent region from 30° to 40°N, 65° to 80°W: (a) before the fall 1982 onset of the countercurrent; (b) just after the fall 1982 onset; (c) just before the fall 1983 onset; (d) after the fall 1983 onset; (e) during the midwinter 1984 slack period;

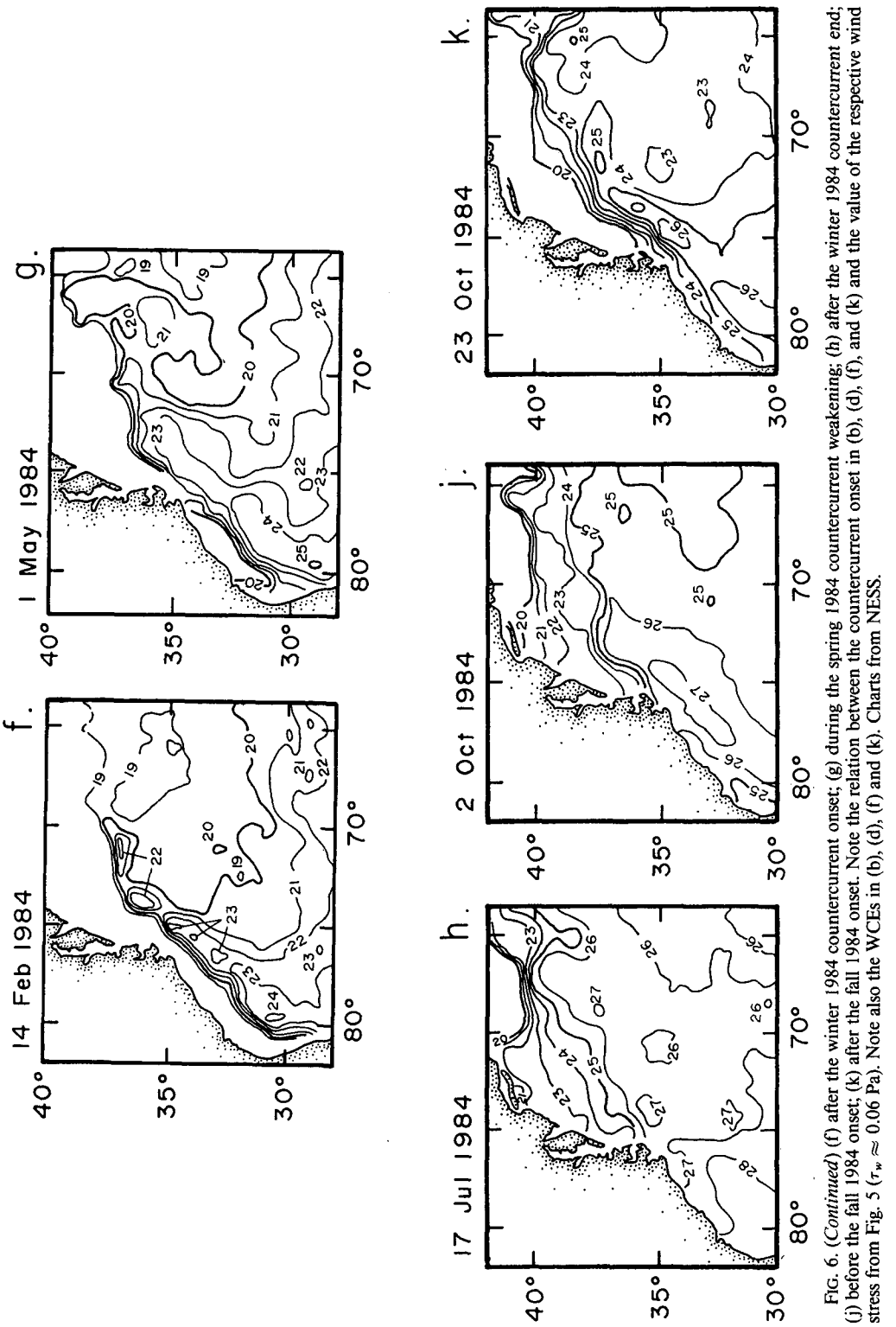

FIG. 6. (*Continued*) (f) after the winter 1984 countercurrent onset; (g) during the spring 1984 countercurrent weakening; (h) after the winter 1984 countercurrent end; (j) before the fall 1984 onset; (k) after the fall 1984 onset. Note the relation between the countercurrent onset in (b), (d), (f), and (k) and the value of the respective wind stress from Fig. 5 ($\tau_w \approx 0.06$ Pa). Note also the WCEs in (b), (d), (f) and (k). Charts from NESS.

the wind and satellite results. One broad peak (December to April) in the wind stress is centered in February. It has a later than usual start, as does the onset of the countercurrent (early December 1982); the onset occurs when the τ_w passes 0.04 Pa. There is no winter lull in τ_w nor any noticeable lessening of the countercurrent. One perplexing result (again) is that the countercurrent persists until the end of July, but τ_w drops below 0.05 Pa in April. The countercurrent returns at the end of October, again when τ_w rises above 0.04 Pa. Further, MS114/S reflects the Bermuda wind more closely than MS114/N, although all are fairly similar; again the curl of τ_w goes as τ_w of MS114/N.

Finally, for 1983–84 (Fig. 5f) we have a more "normal" τ_w and countercurrent pattern; fall and winter peaks, a January lull, a spring weakening and a summer drop-off. As mentioned before, the countercurrent turns on at the end of October and for $\tau_w = 0.04$ Pa, turns off when τ_w drops below 0.07 Pa in the first week of January, turns on again when τ_w rises above 0.09 Pa in the first week of February, diffuses (weakens) when τ_w falls below 0.10 Pa in the first week in May, and ends when τ_w falls below 0.05 Pa in the first week of July. The countercurrent turns on again during the first week of October when τ_w reaches 0.07 Pa, turns off (less distinctly) in the third week of December when τ_w falls below 0.03 Pa, and turns on again (quite distinctly) during the first week of February 1985. The wind data for this last event and the rest of 1985 is not yet available. From a comparison of the monthly wind stress variation for MS114/N and MS114/S, it is not clear for 1983–84 that the curl of τ_w follows τ_w of MS114/N.

For the 1982–84 cases discussed above and presented in Fig. 5e, f, we have presented in Fig. 6a–k ten of the actual satellite SST charts for many of the countercurrent segments. The charts presented cover a two-year period and represent conditions before and after the fall countercurrent onset, during the winter lull, after the winter onset, and after the summer end.

There are four features worth noting here: 1) the countercurrent transitions are abrupt, frequently occurring in one GOSSTCOMP period (seven days) and almost always in less than two weeks; 2) in the January lull period the countercurrent does not diminish to the conditions of summer, but its structure weakens significantly and the February onset is distinct; 3) the spring slackening of the countercurrent is also a less distinct event than are the onsets; and 4) there are always WCEs enclosed within the countercurrent.

In summary, we see from Figs. 3f and 5a a statistical correlation between the wind stress over the interior North Atlantic and the formation of WCEs off Cape Hatteras. Furthermore, from Figs. 5b–f and 6 we observe a direct relation between this wind stress and the onset of a countercurrent south of the Gulf Stream (and its associated WCEs). The countercurrent switches on when the interior wind stress rises above 0.06 $\pm$ 0.02 Pa and, with two springtime exceptions, weakens when the wind stress falls below 0.1 Pa and ceases when it falls below 0.05 $\pm$ 0.02 Pa. Thus, over a period of five years and seven spinup events, there appears to be a single valued relation between the applied force (as approximated by the wind stress) and the acceleration of a countercurrent; we infer a dynamical connection. The dynamical scenario leading to this countercurrent and the WCE formations is discussed in the paragraphs to follow and in section 4b on an instability mechanism. An observable result of the proposed dynamics is that the WCEs off Hatteras become a low-pass anemometer, a Strouhal speedometer, for the interior winds over the North Atlantic; this is a readily testable hypothesis.

In regards to geographic location for the WCE formation, the satellite SST analysis over the last five years for the area east and north of Cape Hatteras (such as shown in Figs. 1 and 6 and Table 1) has been examined. Fifty-five percent of all the GS/S WCEs originate on the Sargasso Sea side of the Gulf Stream at 36.5 $\pm$ 1°N, 69° to 72°W, just downstream from where the stream leaves the continental shelf, as shown in Fig. 1. The Gulf Stream along the shelf up to that point is nearly stationary. Richardson et al. (1978) also observed deep WCEs in this location in June 1975 and April 1977. The present WCEs appear to shed much like eddies downstream from a bluff body; furthermore, at least 25% of them split in two after periods ranging from one week to two months. This generation region is undoubtedly the source for much of the large WCE population of the western North Atlantic that was found in this study.

A similar shedding of CCEs, sometimes called shingles, was observed on the north side of the Gulf Stream by Stumpf and Rao (1975); also, Bane et al. (1981) observed this same phenomenon at a later date. The Stumpf and Rao eddies were 50 to 100 km in size and would be only marginally resolved by the present GOSSTCOMP 50 km analysis. There are indications of them in the January to March period of the present study (particularly the 26 January 1982 chart not presented here), but they do not fulfill our eddy criterion as stated in section 3.

From the preceding description of the temporal and geographic eddy and countercurrent variability we suggest that the wind stress is felt through a spinup of the southern mean current–countercurrent system, and then to finite amplitude lateral instabilities and eddying of this mean current. Local mean current response to the wind stress was observed by Koblinsky and Niiler (1982) in the Atlantic North Equatorial current east of Barbados. This was observed for time scales of four to forty days with the phase lag of the barotropic response being about two weeks. These results are expanded upon in the data from the SEQUAL experiment soon to be published (P. Richardson, private communication); their description now includes the generation of

lateral shear instabilities. The difference in the present proposed wind/current interaction is that here it is not local or weak.

The shedding of WCEs east of Cape Hatteras is the Gulf Stream's response to the seasonal wind stress spinup on the one hand and the inability of the northern part of the gyre to accept a new mean current input on the other. We suggest that initially in the seasonal spinup process, nonlinear advection accelerates the mean Gulf Stream flow up to Cape Hatteras thereby creating a warm core, but then a geostrophic adjustment occurs and establishes a countercurrent. This system becomes unstable and generates WCEs, thus dampening the seasonal signal and preventing it from reaching other parts of the gyre.

Is there evidence that the mean currents of the northern part of the gyre have no seasonal variation? Over the last several years four current meter studies have been published indicating that there is no seasonal modulation north of 37°N or east of 55°W (Hogg et al., 1986; Richardson, 1985; Schmitz, 1980; Luyten, 1977). One of the difficulties in stating this comes from the meandering nature of the mean current in that region, but nevertheless there appears to be no seasonal modulation of the kinetic energy bursts that these current meters see. This data will be discussed further in section 4c on the supporting historical data. In regards to the reason, Luyten (private communication) has suggested that the North Atlantic current system, buoyancy plus wind driven, cannot accept a continuously varying western boundary current input. Perhaps the northern part of the gyre (the "western regime" of Luyten and Stommel, 1986) responds to the seasonal wind stress change via a pressure gradient that sets up the countercurrent and warm core eddying (the "eastern regime" of Luyten and Stommel, 1986). In connection with this it is useful to note from the data of Fig. 3 that all eddies and rings have maximum and minimum formation periods in step with the WCEs. The suggested northern gyre feedback mechanism that produces the countercurrent and WCEs in the Cape Hatteras section of the Gulf Stream might also instigate the meandering and ring formation found in the free stream section north of the Cape.

b. *Instability mechanism*

A less speculative argument can be made regarding lateral barotropic shear instability in the Gulf Stream southern edge/countercurrent regime. This is a logical candidate for finite instability and WCE generation.

Some insight into the dynamics of this potential current/countercurrent eddy generation mechanism is obtained from the instability theory of Pedlosky (1964). Here he establishes that a necessary condition for instability to small disturbances is that the gradient of potential vorticity

$$\frac{dq}{dy} = \beta - \frac{\partial^2 U}{\partial y^2} - \frac{1}{\rho}\frac{\partial}{\partial z}\left(E\rho\frac{\partial U}{\partial z}\right) \quad (1)$$

changes sign somewhere in the flow. This is the β plane equivalent to the inflection point criterion for instabilities in classical shear flows. In the above equation the y-coordinate is cross stream, z is vertically upwards, $U(y)$ the downstream velocity, β the Coriolis parameter, ρ the density, and E a measure of the vertical stratification (smaller E, greater stability). Going from the current to the countercurrent, $\partial^2 U/\partial y^2$ and $\partial^2 U/\partial z^2$ trend from negative to positive, while $\partial U/\partial z$ goes from positive to negative. The relative magnitude of the first two terms of (1) are:

$$\beta = 1.9\times 10^{-13}\ \text{cm}^{-1}\ \text{s}^{-1};$$

$$\frac{\partial^2 U}{\partial y^2} \sim 65\times 10^{-13}\ \text{cm}^{-1}\ \text{s}^{-1} \quad \text{(in stream)}$$

$$\frac{\partial^2 U}{\partial y^2} \sim 30\times 10^{-13}\ \text{cm}^{-1}\ \text{s}^{-1} \quad \text{(countercurrent).}$$

The magnitude of the last term of (1) is difficult to assess because of the effect of gravitational stability; however, the last two terms add to dominate β. These terms cause a sign reversal of (1) in going from the current to the countercurrent; and, consequently, the necessary conditions for lateral barotropic instability are created by the onset of the spring countercurrent.

c. *Supporting historical data for the seasonal variability of the Gulf Stream/countercurrent system*

Seasonal variations in the Gulf Stream transport for 35 sections made between 1932 and 1977 were examined by Worthington (1977), who observed a maximum in the baroclinic transport in April, although there is significant variability at shorter time scales as well. The largest baroclinic transport ever was calculated for the stream in the month of April 1977 from the data of RV *Researcher,* stations 6 and 33 (Worthington, 1977); above 2000 meters it was 95 Sv (Sv $\equiv 10^6\ \text{m}^3\ \text{s}^{-1}$), as opposed to 89 Sv for the Fuglister April 1963 transect and an annual average of 73 Sv from Halkin and Rossby (1985). Almost incidentally from the Worthington study, a strong WCE was also found at 34.4°N, 71.3°W during the April 1977 *Researcher* XBT survey (Worthington, 1977; Richardson et al., 1978). Information on the existence of a countercurrent during this period is not available as only two *Researcher* stations were deep; the rest were XBTs to 760 meters. If additional data could be found, the spring of 1977 would probably prove to be a significant time for WCE formation. A more recent investigation of seasonal variations in the Gulf Stream over a 2½ year period is found in Halkin and Rossby (1985). They find at 73°W a maximum in the total Gulf Stream transport in March. The March value is 140% of the mean with the shorter term variability amounting to

20% of the mean. Perhaps this shorter term variability is caused by the shedding of eddies.

Another, and for our purposes more relevant, study of the seasonal variability of the Gulf Stream was done by Fu et al. (1987). His (highly massaged) altimetry data for the period 1975 to 1978 shows a seasonal variability of the cross-stream sea level difference of 15 cm, or 15% assuming a 1 meter mean difference. Of more interest here, however, is the data for the year 1977/78; the mean surface transport exhibits maxima at the end of October and April with minima in December and August. This bimodal pattern is quite similar to what we found in the present study for the wind stress, the countercurrent onset, and WCE formations in the years 1980/81 and 1983/84.

With regard to the Gulf Stream spring forcing that might lead to instabilities, Fuglister (1963) determined the dynamic height change across the stream during April 1960; the dynamic height was calculated between 200 and 4000 meters depth. There was the expected 1.2 meter increase as he went south along 60°30′W, but then there was a 0.25 meter drop between 37° and 36°N indicating a spring countercurrent. Associated with this dynamic height change was the geostrophic Gulf Stream transport between 37° and 38°20′N of 137 Sv and a countercurrent between 37° and 33°N of 68 Sv. This Gulf Stream transport is 20% higher than average, and the current/countercurrent region represents a significant source of energy for shear instability, which was explored in section 4b. A similar but weaker change in dynamic height was seen on the northern edge of the Gulf Stream indicating a countercurrent there as well.

The specific historical evidence for the existence of a deep, seasonal countercurrent is sketchy but encouraging. Schmitz (1980) reported the first direct evidence for the recirculation along 55°W. From the POLYMODE 2 array current meter data taken along 55°W from 1975 to 1977 he observed at 30°N a 6 to 10 cm s^{-1} westward current. It was from 600 meters to 4000 meters in depth and 200 km wide. The south side of the eastward flowing Gulf Stream and this westward jet were nearly barotropic; however, no seasonal modulation was reported for this longitude. Indeed, as mentioned previously, the shedding of WCEs may block the seasonal signal from reaching this far east. Richardson (1985), using current meter, surface drifter, and float data along 55°W, reports a countercurrent along both sides of the Gulf Stream. A baroclinic countercurrent, also along both sides of the Gulf Stream, is frequently reported further west, for instance in the previously mentioned Fuglister (1963) section at 60°30′ taken during April. In this data a warm core of +5°C surface water is observed extending northward between the stream and the interior and positioned over a baroclinic countercurrent, which extends down to 4000 meters. This section was taken in April of 1960 and shows, in addition to the countercurrent, deep eddylike perturbations of the isotherms.

The seasonal nature of the countercurrent and eddying is suggested in the Fuglister (1960) transects of Fig. 7, as well as in the Worthington (1976) sections. These four datasets are cross sections of the Gulf Stream from Cape Hatteras to the Sargasso Sea interior, two taken in the spring and two in the early summer. Figure 7a is the 19–26 April 1959 Fuglister section along 36°N; it shows a +6°C warm core of surface water with a baroclinic countercurrent/eddy structure beneath it to 4000 meters. The 9–14 June 1955 section of Fig. 7b is from Hatteras to Bermuda; it shows a broad +3°C warm tongue confined to the upper 200 meters. The Worthington (1976) transects off Cape Hatteras reveal a similar pattern. The March 1957 cross section reveals a +5°C warm core with a baroclinic countercurrent/eddylike structure down to 4000 meters, whereas the June 1966 cross section has a broad shallow +2°C warm tongue confined to the upper 200 meters.

The deep seasonal nature of eddying off Cape Hatteras is further supported by the 4000 meter current meter records of Luyten (1977) taken at 36°30′N, 69°30′W for the period April through December 1974. Although the period is limited to eight months, Luyten's Fig. 9 clearly shows intense bursts of eddy energy that start at the beginning of the record and last until July. There are four or five eddy events occurring between April and July with only weaker fluctuation, perhaps meandering, occurring afterwards from July through November. Similar activity, potentially of a seasonal nature, is found in the short 1970 current meter results (taken at 35°59′N, 70°37′W) that Luyten presents in his Fig. 12. These records are from December 1970 through July 1971, and show weak variability of order 10 cm s^{-1} up to the middle of February, followed by stronger 30 cm s^{-1} bursts from 15 February through 27 July. This contrasts with the current meter records of Hogg et al. (1986, their Fig. 2) of the northern Gulf Stream and its recirculation gyre (at 40°N, 60°W). No seasonal modulation of the velocity (eddy) bursts are observed at this location. Furthermore, as the many LOTUS data reports show (at 34°N, 70°W), there is little evidence of seasonal eddy burst activity at this location either.

5. Conclusion

Eddy SST tracking by satellite requires relative temperature accuracy, not absolute. With the multiple-channel AVHRR on the NOAA-7 polar orbiting satellites, great improvements have been made in spatial and temperature resolution, as well as in cloud discrimination and water vapor correction since POLYMODE. Furthermore, although individual satellite SST snapshots can be misleading, observing the weekly eddy movement and establishing thresholds in temperature

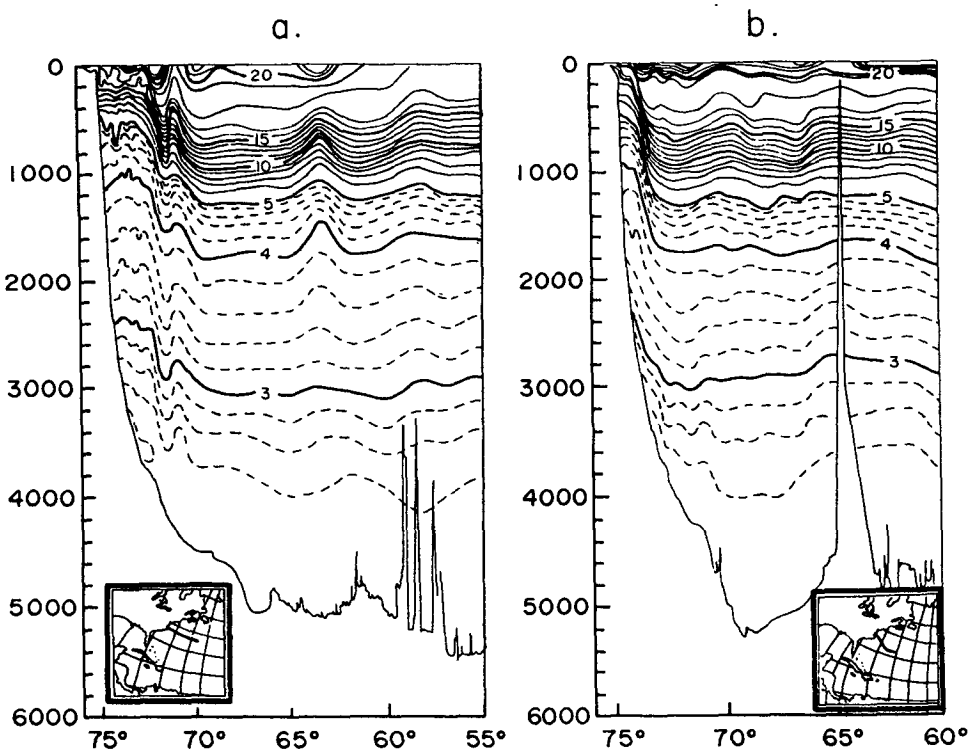

FIG. 7. Cross sections of the Gulf Stream in the spring and summer showing the countercurrent and its absence. (a) Transect from Cape Hatteras (inset), 19–26 April 1959 showing the countercurrent and eddies down to 4000 meters. (b) Transect from Cape Hatteras (inset), 9–14 June 1955, showing virtually no countercurrent or warm surface core (from Fuglister, 1960).

defect, size, and time greatly improve the eddy resolution. Satellite SST data and the GOSSTCOMP 50 km analysis can now provide reliable statistics on coherent eddy formation in the western North Atlantic, although the eddy lifetimes are surely underestimated.

The present study reproduces in the POLYMODE area and time frame the same number of medium to strong eddies as were seen earlier by POLYMODE in 1978–79; the results are also in general agreement with other more contemporary but limited studies. The GOSSTCOMP analysis used here reveals a broad diversity as to type and number of eddies and has been used to keep a continuing count on eddy formation in the western North Atlantic.

The concentration of WCE formation in the late fall and late winter/spring with a midwinter dip and just downstream of where the Gulf Stream leaves the shelf indicates possible Gulf Stream–countercurrent finite instability as an eddy generation mechanism. This is motivated from the analysis of the gyre interior wind stress for the same period, as well as from the results of stability analysis of the current/countercurrent flow. That this mechanism is responsible for the insensitivity of the northern part of the gyre to seasonal wind stress variation is postulated and reinforced with historical data. Finally, the overall coherent eddy distribution in space and time suggests the possibility of developing satellite-derived regional eddy diffusivities for use in general circulation models; the eddy density near the Gulf Stream has a large seasonal fluctuation.

Acknowledgments. I would like to thank Herman Bosch, Tom Bolmer, and Roger Goldsmith for their help with the wind stress data.

REFERENCES

Bane, J. M., Jr., D. A. Brooks and K. Lorenson, 1981: Synoptic observations of the three-dimensional structure and propagation of Gulf Stream meanders along the Continental margin. *J. Geophys. Res.*, **86**, 6411–6425.

Brower, R., 1976: Satellite-derived sea surface temperature from NOAA spacecraft. NOAA Tech. Memo., NESS No. 78, Washington, DC.

Brown, O., D. Olson, J. Brown and R. Evans, 1984: Kinematics of a Gulf Stream warm core ring. *Aust. J. Mar. Freshwater Res.*, **34**, 535–545.

Bunker, A., and R. Goldsmith, 1979: Archived time series of Atlantic Ocean meteorological variables and surface fluxes. Woods Hole Oceanographic Institution Tech. Rep. 79-3, 27 pp.

Cornillon, P., D. Evans and W. Large, 1986: Warm outbreaks of the Gulf Stream into the Sargasso Sea. *J. Geophys. Res.*, **91**(C5), 6583–6596.

Cox, S., 1982: Satellite applications to acoustic prediction system. M.S. thesis, Naval Postgraduate School.

Dickson, R., W. Gould, P. Gurbett and P. Kilworth, 1982: A seasonal

signal in ocean currents to abyssal depths. *Nature,* **295,** 193–198.

Emery, W., C. Ebbesmeyer and J. Dugan, 1980: The fraction of vertical isotherm deflections associated with eddies: An estimate from multiship XBT surveys. *J. Phys. Oceanogr.,* **10,** 885–899.

——, A. Thomas, M. Collins, W. Crawford and D. Mackas, 1986: Comparison between satellite image advective velocities, dynamic topography, and surface drifter trajectories. *Eos,* **67**(22), 498.

Fu, L., J. Vazques and M. Parks, 1987: Seasonal variability of the Gulf Stream from satellite altimetry. *J. Geophys. Res.,* **92**(C1), 749–754.

Fuglister, F. C., 1960: *Atlantic Ocean Atlas.* Vol. 1, Woods Hole Oceanographic Institution, Atlas Ser., 209 pp.

——, 1963: Gulf Stream '60. *Progress in Oceanography,* Vol. 1, Pergamon, 267–373.

Gotthardt, G., and G. Potocsky, 1974: Life cycle of a Gulf Stream anticyclonic eddy observed from several oceanographic platforms. *J. Phys. Oceanogr.,* **4,** 131–134.

Halkin, D., and T. Rossby, 1985: The structure and transport of the Gulf Stream at 73°W. *J. Phys. Oceanogr.,* **15,** 1439–1452.

Hardtke, P. G., and J. Meincke, 1984: Kinematical interpretation of infrared surface pattern in the North Atlantic. *Oceanol. Acta,* 7(3), 373–378.

Hogg, N., R. Pickart, R. Hendry and W. Smethie, 1986: The northern recirculation gyre of the Gulf Stream. *Deep-Sea Res.,* **33**(9A), 1139–1165.

Ikeda, M., L. Mysak and W. Emery, 1984: Observation and modeling of satellite-sensed meanders and eddies off Vancouver Island. *J. Phys. Oceanogr.,* **14,** 3–21.

Joyce, T., 1984: Velocity and hydrographic structure of a Gulf Stream warm core ring. *J. Phys. Oceanogr.,* **14,** 936–947.

Koblinsky, C., and P. Niiler, 1982: The relationship between deep ocean currents and winds east of Barbados. *J. Phys. Oceanogr.,* **12,** 144–153.

Luyten, J., 1977: Scales of motion in the deep Gulf Stream and across the Continental Rise. *J. Mar. Res.,* **35**(1), 49–74.

——, and H. Stommel, 1986: Gyres driven by combined wind and buoyancy flux. *J. Phys. Oceanogr.,* **16**(9), 1551–1560.

Maul, G., and N. Bravo, 1983: Fitting of satellite and in situ ocean surface temperatures: Results for POLYMODE during the winter of 1977–78. *J. Geophys. Res.,* **88,** 9605–9616.

Müller, P., 1983: Evidence for the direct forcing of midocean eddies. *Proc. Conf. on Eddy Contrib. to General Circulation,* University of Hawaii.

Pedlosky, J., 1964: The stability of currents in the atmosphere and ocean. Part I. *J. Atmos. Sci.,* **21,** 201–219.

POLYMODE XBT Group, 1978: POLYMODE XBT surveys. PM XBT Tech. Reps. 78-10, 78-11, 78-12, 78-13 and 78-14, Woods Hole Oceanographic Institution.

——, 1979: POLYMODE XBT surveys. PM Tech. Reps. 79-3, 79-4, 79-5, 79-6, and 79-9, Woods Hole Oceanographic Institution.

Richardson, P., 1983: Eddy kinetic energy in the North Atlantic from surface drifters. *J. Geophys. Res.,* **88**(C7), 4355–4367.

——, 1985: Average velocity and transport of the Gulf Stream near 55°W. *J. Mar. Res.,* **43**(83), 111.

——, R. Cheney and V. Worthington, 1978: A consensus of Gulf Stream rings, spring 1975. *J. Geophys. Res.,* **83,** 6136–6144.

Ring Group, 1981: Gulf Stream cold core rings: Their physics, chemistry, and biology. *Science,* **212,** 1091–1100.

Schmitz, W., 1980: Weakly depth-dependent segments of the North Atlantic circulation. *J. Mar. Res.,* **38**(1), 111–133.

Seaver, G., 1979: Eddy sea surface temperature by ship and satellite. *POLYMODE News* 70, 17 August 1979.

Strong, A., and P. McLain, 1984: Improved ocean surface temperatures from space—comparison with drifting buoys. *Bull. Amer. Meteor. Soc.,* **65,** 138–142.

——, A. Gruber and L. Stowe, 1982: Effects of El Chichón eruptions on satellite observation. NASA Tech. Memo. 84959, 4-1 to 4-11.

Stumpf, H., and P. Rao, 1975: Evolution of Gulf Stream eddies as seen in satellite infrared imagery. *J. Phys. Oceanogr.,* **5,** 388–393.

Tabata, S., and J. Gower, 1980: A comparison of ship and satellite measurements of sea surface temperature off the Pacific coast of Canada. *J. Geophys. Res.,* **85,** 6636–6648.

Thompson, R., 1984: A cyclonic eddy over the continental margin of Vancouver Island: Evidence for baroclinic instability. *J. Phys. Oceanogr.,* **14,** 1326–1348.

Worthington, V., 1976: *On the North Atlantic Circulation. The Johns Hopkins Oceanogr. Stud.,* No. 6, 110 pp.

——, 1977: Intensification of the Gulf Stream after the winter of 1976–77. *Nature,* **270,** 415–417.